Petroleum 6 (2020) 106–113

Contents lists available at ScienceDirect

Petroleum

journal homepage: http://www.keaipublishing.com/en/journals/petroleum

CO_2 corrosion behaviors of 13Cr steel in the high-temperature steam environment

Guoqing Xiao[a,b,*], SiZhou Tan[a], Zhiming Yu[b], Baojun Dong[b], Yonggang Yi[c], Gang Tian[c], Huiyong Yu[c], Shanzhi Shi[c]

[a] College of Chemical Engineering, Southwest Petroleum University, Chengdu, 610500, China
[b] State Key Laboratory of Oil & Gas Reservoir Geology and Exploitation (Southwest Petroleum University), Chengdu, 610500, China
[c] Research Institute of Engineering Technology, Xinjiang Oilfield Company, PetroChina, Karamay, 834000, China

ARTICLE INFO

Keywords:
CO_2 auxiliary steam drive
Temperature
Cl^- concentration
Corrosion
13Cr steel

ABSTRACT

The study aims to explore the corrosion behaviors of 13Cr steel in the high-temperature steam environment. The corrosion behaviors of 13Cr steel were tested in CO_2 auxiliary steam drive environment simulated with the HTHP autoclave. The corrosion morphology and product composition were explored by SEM, EDS, XRD and XPS. The exploration results showed the corrosion rate of 13Cr steel in the high-temperature steam environment was less than 0.04 mm/a. The corrosion behaviors of 13Cr steel were mainly affected by temperature and chloride ion concentration. Temperature inhibited steam condensation and the compactness of Cr-rich layer. With the increase in temperature, more droplets were adsorbed on the surface of 13Cr steel and the compactness of the Cr-rich layer is worse. Chloride ions affects the activity of Fe atoms in the metal matrix. When chloride concentration increased, Fe^{2+} concentration in the solution and $FeCO_3$ content in the rich-Cr layer were increased and the rich-Cr layer became looser.

1. Introduction

Industrial CO_2 emissions largely lead to global warming. At present, the main technology of emission reduction is CCUS (carbon capture, utilization and storage). Currently, CCUS is mainly applied in CO_2-EOR drive recovery. CO_2-EOR enhanced oil recovery technology not only reduces CO_2 emissions, but also increases the recovery rate of oil fields [1,2].

The viscosity of heavy oil in heavy oil reservoir formation can be decreased by injecting steam and a small quantity of CO_2 into gas wells. During steam injection, the wellbore temperature (160–220 °C) of gas injection wells is high and injected CO_2 cools the wellbore to generate the water film on the inner wall of wellbore [3]. When steam injection stops, the temperature of wellbore gradually decreases and the water film is formed on the inner wall of wellbore. When CO_2 is dissolved in water, carbonic acid is formed. Carbonic acid significantly increases the corrosion rate of tubing and casing steel and causes sweet corrosion [4,5]. The safe storage of CO_2 problem in gas injection wells remains to be solved. According to the study results of the Kawasaki Heavy Industries and Sumitomo Metal Industries, when the temperature was higher than 180 °C, stainless steel (22Cr and 25Cr steel) containing the higher level of Cr should be adopted [6].

In previous studies on CO_2 corrosion of 13Cr steel, only the water-phase environment was usually considered, but the effect of steam on corrosion was seldom explored [7–9]. However, the injected medium is usually a mixture of steam and CO_2. The steam is one of the important factors affecting the corrosion behavior of the system. Therefore, if the materials recommended in the wellbore specifications were adopted, overestimated corrosion damage and high cost would be generated.

13Cr steel is widely used in oil and gas industry due to its good corrosion resistance. The main factors influencing CO_2 corrosion of 13Cr steel are temperature, CO_2 partial pressure, velocity and Cl^- ion concentration [10]. The corrosion behaviors of 13Cr steel were extensively studied. Hua pointed that the general corrosion rate of 13Cr steel was less than 0.02 mm/a in water-saturated supercritical CO_2 environments with SO_2/O_2 [11]. However, the CO_2 corrosion behaviors in the high-temperature steam environment were seldom explored [12,13].

The study aims to explore the corrosion behaviors of 13Cr steel in the high-temperature steam environment. The corrosion behaviors of 13Cr steel were tested in CO_2 auxiliary steam drive environment simulated with the HTHP autoclave. In addition, the CO_2 corrosion

Peer review under responsibility of Southwest Petroleum University.
* Corresponding author. College of Chemical Engineering, Southwest Petroleum University, Chengdu, 610500, China.
E-mail address: gqxiao68@sina.com (G. Xiao).

https://doi.org/10.1016/j.petlm.2019.12.001
Received 3 September 2019; Received in revised form 16 September 2019; Accepted 16 December 2019

Table 1
Chemical composition of 13Cr steel (wt.%).

Steel	C	Mn	Cr	Ni	Cu	P	Si	Fe
13Cr	0.22	0.75	13	0.5	0.25	0.02	1.00	Bal.

mechanism in the high-temperature steam environment was discussed, thus providing the basis for the application of 13Cr steel in gas injection.

2. Experiments

2.1. Materials and solutions

The 13Cr steel was selected as the experimental material. The chemical composition of 13Cr steel specimen is listed in Table 1. According to the ASTM standards, the testing specimens were machined into a size of 30 × 15 × 3 mm. The surface of each specimen was polished with 1200# silicon sandpaper to eliminate scratches. The polished specimens were cleaned with anhydrous ethanol, degreased with acetone, finally dried in the air and stored in the desiccator for 2 h. The weight of the specimen was taken using an analytical balance with the accuracy of 0.1 mg.

The experimental medium was deionized water. Before the experiment, purified CO_2 was bubbled into deionized water to purge oxygen for 12 h.

2.2. Weight loss test

The experiments were conducted in a self-machined HTHP autoclave (Fig. 1). Firstly, 60 mL of deoxidized deionized water was added into the autoclave. The specimens were hung on the specimen holders, which were then placed above the liquid level. The autoclave was sealed and purged with CO_2 for 2 h at a low flow rate. The experiment temperature and flow rate were respectively set after oxygen removal. When the experimental temperature raised to the required temperature, CO_2 was purged into the autoclave by using a booster pump. The corrosion experiments were performed for 72 h.

After corrosion experiments, four parallel specimens were taken out from the autoclave. The three specimens were cleaned immediately by deionized water followed with alcohol. The corrosion products were removed according to ASTM Standard G1-03. Then the specimens were weighed on an electronic balance with the precision of 0.1 mg. The general corrosion rates were calculated with Eq. (1) [14].

$$v = 87600\frac{\Delta m}{\rho A \Delta t} \quad (1)$$

where v is corrosion rate (mm/a); Δm is the weight loss (g); ρ is the density of steel (g/cm^3); A is the surface area (cm^2); Δt is corrosion time (h).

The other specimen was washed with deionized water, dehydrated with alcohol, and dried in air. The surface morphology of the dried specimen was analyzed with SEM (JSM-7500F) and its chemical composition of the corrosion scale was determined with XRD (XPert Pro MPD) and XPS (Phi-Quantera II).

Table 2
Test conditions.

Temperature (°C)	CO_2 partial pressure (MPa)	Flow rate (m/s)	chloride ion content (ppm)	Experimental medium	Test time (h)
160	2	–	–	deionized water	72
180	2	–	–	–	72
200	2	–	–	–	72
220	2	–	–	–	72
160	1	–	–	–	72
160	3	–	–	–	72
160	4	–	–	–	72
160	2	3	–	–	72
160	2	4.5	–	–	72
160	2	6	–	–	72
160	2	–	1000 ppm	Formation water	72
160	2	–	2000 ppm	Formation water	72
160	2	–	3000 ppm	Formation water	72

2.3. Testing scheme

The main corrosion factors of injection wells were temperature, CO_2

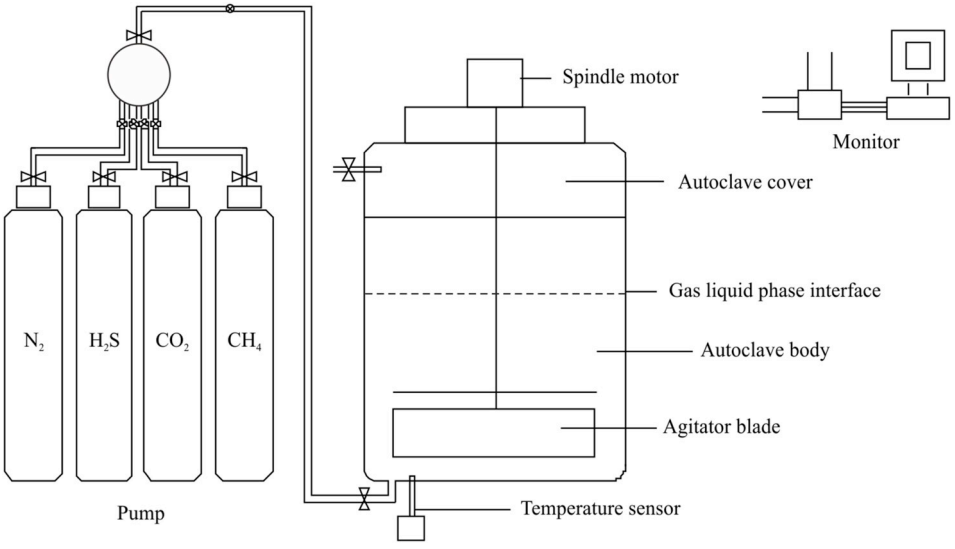

Fig. 1. Schematic diagram of dynamic HTHP autoclave.

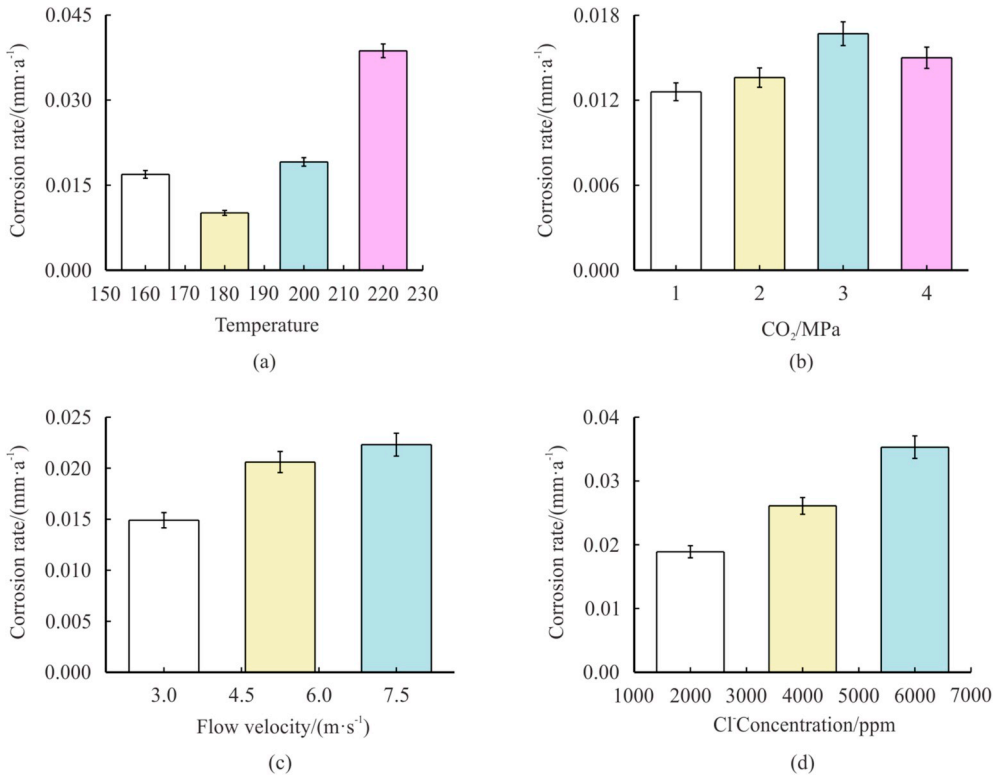

Fig. 2. Corrosion rates of 13Cr steel.

pressure, flow rate and chloride ion content. According to the statistical data of gas injection wells, the experimental scheme is listed in Table 2.

3. Results

3.1. Weight loss corrosion rate

Fig. 2 shows the corrosion rates of 13Cr steel at various temperatures. The corrosion rates of 13Cr steel were lower than 0.04 mm/a, indicating that 13Cr steel had the good corrosion resistance. Among all the corrosion factors, temperature and Cl^- content had a great influence on the corrosion of 13Cr steel (Fig. 2).

3.2. SEM observation and EDS analysis

Fig. 3 shows the SEM images (×100) of 13Cr steel at various temperatures. From Fig. 3a–d, the corrosion of specimen was slight. The circled corrosion products appeared on the surface of specimens. As the temperature increased, the corrosion products on the surface of specimens increased.

Fig. 4 shows the SEM images (×10000) of 13Cr steel at various temperatures. The corresponding EDS results are provided in Table 3. From Fig. 4, the circular corrosion products were scattered on the specimen surface. The compact and integrated corrosion scales covered the specimen surface. The cubic corrosion products were existed on the surface of specimen. The corrosion products mainly included $FeCO_3$ and $Cr(OH)_3$, as indicated in the XPS analysis results in Fig. 8. The Cr content of corrosion products was slightly higher than that in the metal matrix.

Fig. 5 shows the SEM images (×100) of 13Cr steel under various chloride concentrations. The corrosion of specimens was slight. The scratches on the specimen surface were obvious. When the chloride ion concentration was 3000 ppm, many corrosion products were observed on the specimen surface.

Fig. 6 was the SEM images (×10000) of 13Cr steel under different flow rate. Corrosion scales were damaged. Cubic crystals occurred on the specimen surface. EDS and XPS results indicated that the cubic crystals were $FeCO_3$.

3.3. XRD analysis

Fig. 7 shows the XRD results of steel. Only Fe peaks were detected. Xu also pointed out that these base metal peaks were detected because the layer formed on the steel surface was thin. Xu reported similar results that the corrosion scales of steel were thin in the high-temperature steam environment [10].

3.4. XPS analysis

To further confirm the chemical composition of corrosion scales, the XPS test was conducted with the specimen. Fig. 8 shows the XPS result of 13Cr steel under conditions (160 °C and 2 MPa CO_2). The O peaks at 530.7 ev and 531.8 ev (Fig. 8a) were ascribed to O^{2-} components. The O1s peak was related to the presence of $FeCO_3$, Fe_2O_3, and Cr_2O_3 [15]. The C peak at 289.6 ev corresponded to adventitious carbon (Fig. 8b). A couple of $Cr2p_{3/2}$ (577.3 ev) and $Cr2p_{1/2}$ (587.1 ev) peaks were ascribed to $Cr(OH)_3$ and Cr_2O_3 (Fig. 8c). A pair of $Fe2p_{3/2}$ and $Fe2p_{1/2}$ peaks at 724.02 ev, 710.61 ev were observed (Fig. 8d). The XPS results of 13Cr steel indicated that the main components of the passive film were $FeCO_3$, Fe_2O_3, $Cr(OH)_3$, and Cr_2O_3.

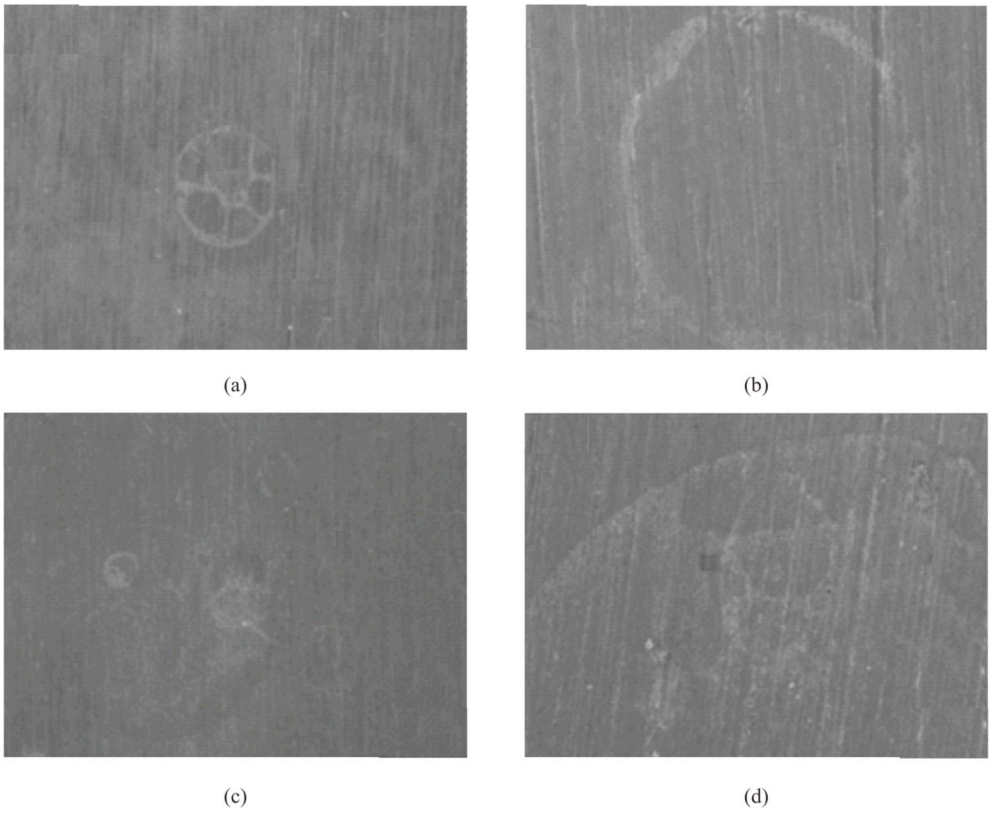

Fig. 3. SEM images (×100) of 13Cr steel at various temperatures. (a: 160 °C; b: 180 °C; c: 200 °C; d: 220 °C).

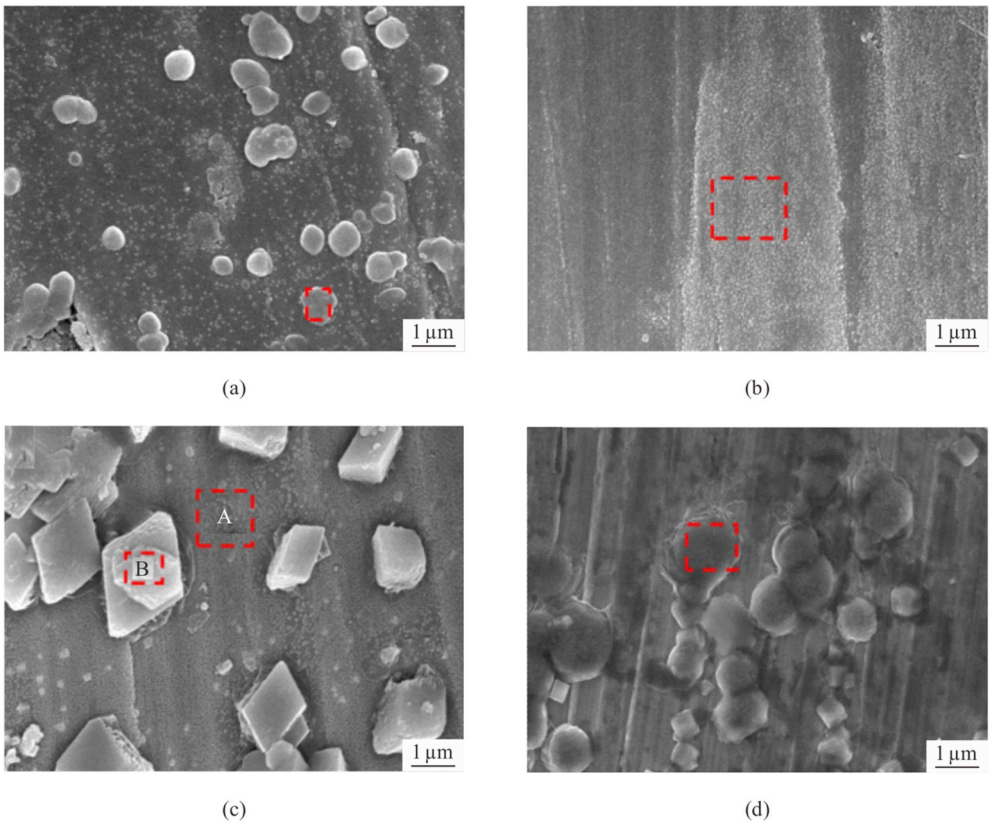

Fig. 4. SEM image (×10000) of 13Cr steel at various temperatures. (a: 160 °C; b: 180 °C; c: 200 °C; d: 220 °C).

Table 3
EDS results of 13Cr Steel at different temperatures.

Temperatures	Elements					
	Zones	C	O	Si	Cr	Fe
160 °C		7.28	6.48	0.71	15.02	70.51
180 °C		4.72	3.06	0.61	14.16	72.88
200 °C	Zone A	3.95	2.06	0.06	10.79	75.26
	Zone B	3.95	2.06	0.06	15.21	73.26
220 °C		4.62	4.40	–	14.19	77.20

4. Discussions

4.1. Corrosion reactions of 13Cr steel

During the corrosion of 13Cr steel in a high-temperature steam environment containing CO_2, water was first absorbed on the steel surface to form a thin water film.

CO_2 is dissolved in water film to form H_2CO_3 (Eq. (2)). H_2CO_3 is further decomposed to generate HCO_3^-, CO_3^{2-} and H^+. Cathodic reactions of the water film are provided as Eq. (3)- Eq. (5) [16,17].

$$CO_2(g) + H_2O \rightarrow H_2CO_3 \quad (2)$$

$$2H_2CO_3 + 2e^- \rightarrow 2HCO_3^- + H_2 \quad (3)$$

$$2HCO_3^- + 2e^- \rightarrow 2CO_3^{2-} + H_2 \quad (4)$$

$$2H^+ + 2e^- \rightarrow H_2 \quad (5)$$

Anodic reactions involve the iron dissolution (Eq. (6) and Eq. (7)):

$$Fe \rightarrow Fe^{2+} + 2e^- \quad (6)$$

$$Cr \rightarrow Cr^{3+} + 2e^- \quad (7)$$

XPS results showed that the corrosion products were mainly $FeCO_3$, $Cr(OH)_3$, Fe_2O_3 and Cr_2O_3. The Ksp of $Cr(OH)_3$ was much lower than that of $FeCO_3$, so $Cr(OH)_3$ rapidly reached the saturation state and amorphous $Cr(OH)_3$ was formed on the surface of substrate (Eq. (8)-Eq. (9)) [18]:

$$Cr^{3+} + 3H_2O \rightarrow Cr(OH)_3 + 3H^+ \quad (8)$$

$$2Cr(OH)_3 \rightarrow Cr_2O_3 + 2H_2O \quad (9)$$

H^+ ion is produced by the hydrolysis of Cr, thus reducing the pH value of the solution and promoting the rapid dissolution of Fe^{2+}. Lots of Fe^{2+} accumulates in the amorphous $Cr(OH)_3$ layers. When the contents of Fe^{2+} and CO_3^{2-} are above the solubility of $FeCO_3$, will $FeCO_3$ precipitates on steel surface (Eq. (10)-Eq. (12)). According to Chen's report, when the Cr content in steel exceeded 3%, a Cr-rich layer was formed on the surface of steel. The formation of $Cr(OH)_3$ decreased the pH value of the solution near the Cr-rich layer, further accelerating the dissolution of $FeCO_3$.

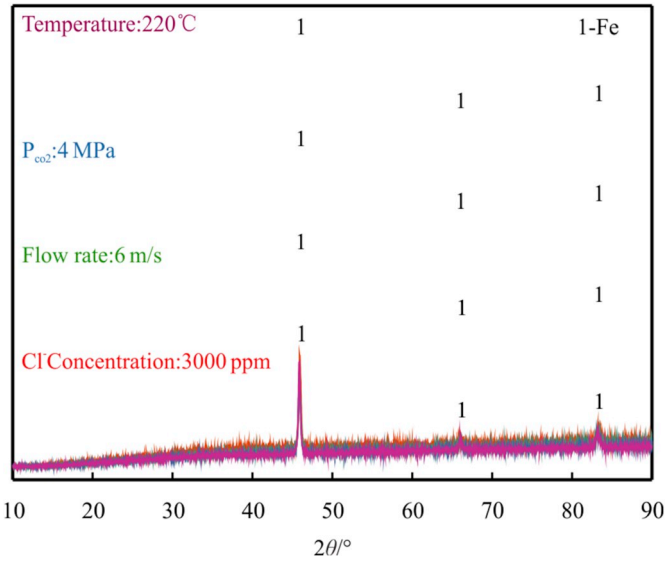

Fig. 7. XRD spectra of corrosion films of 13Cr steel.

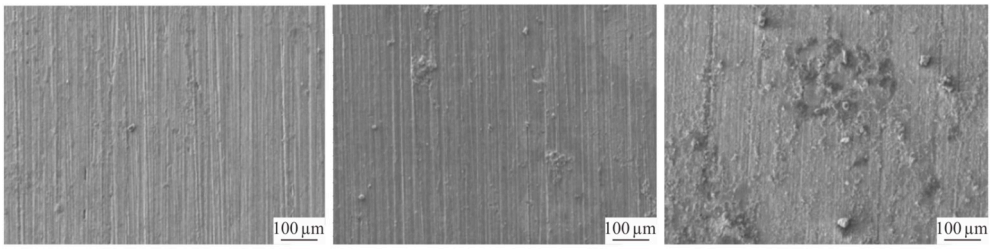

Fig. 5. SEM images (×100) of 13Cr steel under different chloride concentrations. (a:1000 ppm; b: 2000 ppm; c: 2000 ppm).

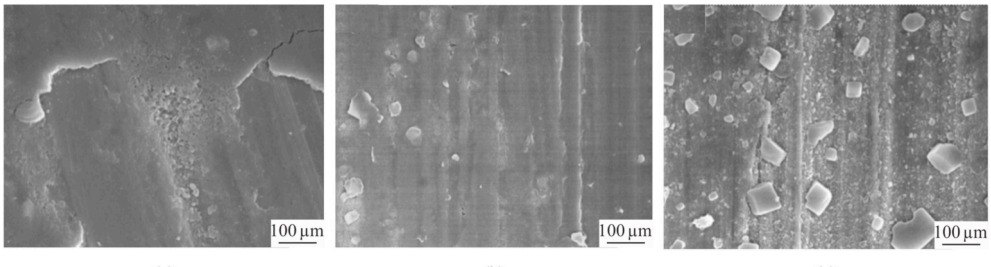

Fig. 6. SEM images (×100) of 13Cr steel under different flow rate. (a: 3 m/s; b: 4.5 m/s; c: 6 m/s).

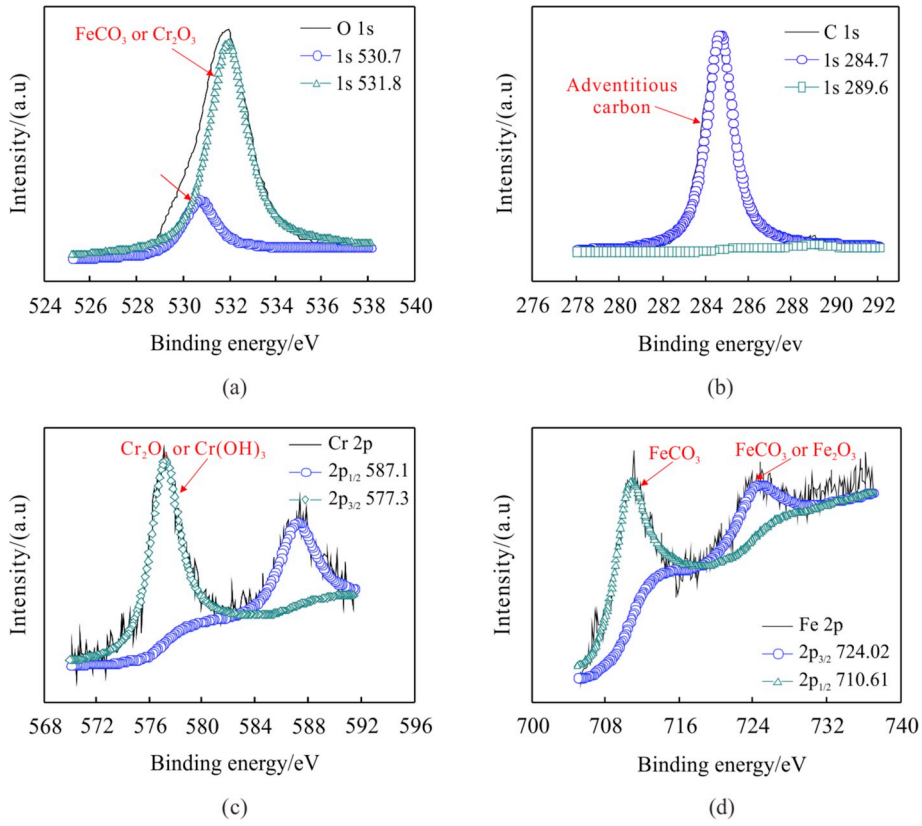

Fig. 8. XPS of 13Cr steel after corrosion at 160 °C under 2 MPa CO_2: (a) o, (b) C, (C) Cr, (d) Fe.

$$Fe^{2+} + CO_3^{2-} \rightarrow FeCO_3 \quad (10)$$

$$Fe^{2+} + 2HCO_3^- \rightarrow Fe(HCO_3)_2 \quad (11)$$

$$Fe(HCO_3)_2 \rightarrow FeCO_3 + CO_2 + H_2O \quad (12)$$

$FeCO_3$ was decomposed into FeO at high temperature (Eq. (13)). When the specimens were taken out from the autoclave, FeO were oxidized in the air to form Fe_2O_3 (Eq. (14)). Cr_2O_3 was generated from the dehydration of $Cr(OH)_3$ (Eq. (15)).

$$FeCO_3 \rightarrow FeO + CO_2 \quad (13)$$

$$4FeO + O_2 \rightarrow 2Fe_2O_3 \quad (14)$$

$$2Cr(OH)_3 \rightarrow Cr_2O_3 + 2H_2O \quad (15)$$

4.2. Influence of temperature

When the steam was cooled, it was condensed on the specimen surface. The specimens were corroded at the condensed area. With the temperature increase, corrosion products on the specimen increased, indicating that temperature affected the quantity of adsorbed water on the specimen surface. Steam absorbed a lot of heat during the condensation process. The higher temperature resulted in more condensed steam on the specimen surface.

Lin indicated that the formation of the Cr-rich layer was ascribed to the competition between $Cr(OH)_3$ and $FeCO_3$. Fig. 9 shows the influence of temperature on the corrosion of 13Cr steel. Temperature mainly affected the ratio of $Cr(OH)_3$ to $FeCO_3$ in the Cr-rich layer. The solubility of $Cr(OH)_3$ ($K_{sp} = 6.3 \times 10^{-31}$) was far less than that of $FeCO_3$

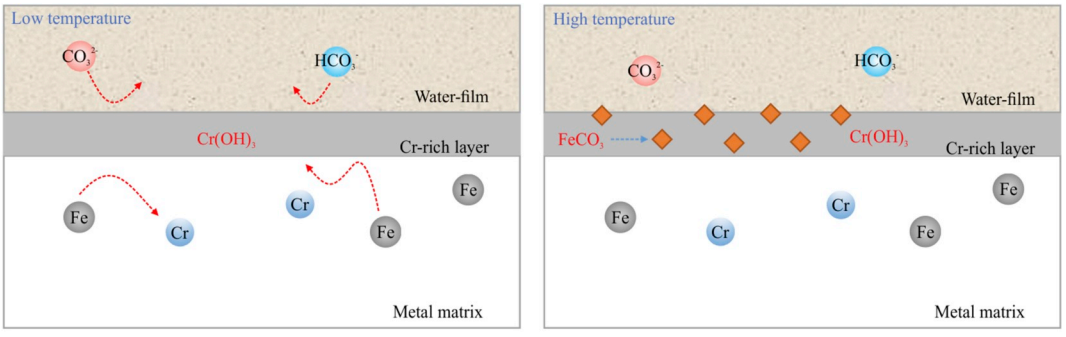

Fig. 9. Influence of temperature on the corrosion of 13Cr steel.

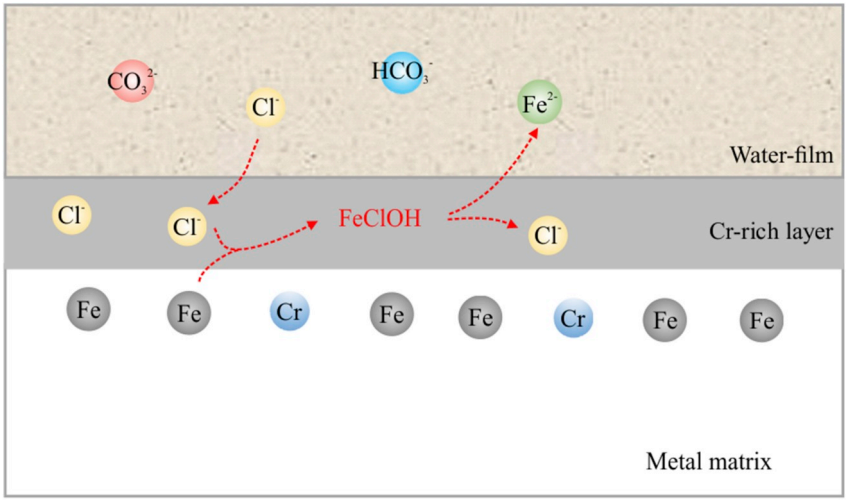

Fig. 10. Schematic diagram of chloride ion activation mechanism.

($K_{sp} = 3.13 \times 10^{-11}$). The content of $Cr(OH)_3$ in the Cr-rich layer was much higher than that of $FeCO_3$ at low temperature [19]. The Cr-rich layer could prevent anions such as CO_3^{2-} and HCO_3^- from penetrating through the Cr-rich layer to react with the matrix. The Cr-rich layer could also inhibit the active dissolution of Fe [20]. The active dissolution of Fe would be accelerated at the high temperature. The content of $FeCO_3$ in the Cr-rich layer increased. $FeCO_3$ crystals would be formed on the surface of the Cr-rich layer and inside the layer.

4.3. Influence of chloride ion concentration

Zhang pointed out that the increase in chloride ion concentration led to the enhanced conductivity of the solution, which increased chloride ions adsorbed on the specimen surface. Moreover, chloride ions reacted with iron ions to generate compounds, which promoted the active dissolution of Fe.

Fig. 10 shows the schematic diagram of chloride ion activation mechanism. Chlorine ions reacted with Fe atoms to form FeClOH, which was easily decomposed into Fe2+ and chloride ions. Due to the activation of chloride ions, Fe atoms easily became Fe2+. With the increase in chloride ion concentration, more Fe^{2+} ions were generated in the water film and the content of $FeCO_3$ in the Cr-rich layer also increased. $FeCO_3$ crystals would be formed on the surface of the Cr-rich layer and inside the layer.

5. Conclusions

(1) The corrosion rate of 13Cr steel in the high-temperature steam environment was less than 0.04 mm/a, it decreases first and then increases with the increase of temperature, and increases with the increase of Cl-concentration. The corrosion behaviors of 13Cr were mainly affected by temperature and chloride ion concentration.
(2) Temperature inhibited steam condensation and the compactness of Cr-rich layer. With the increase in temperature, more droplets were adsorbed on the surface of 13Cr steel and the compactness of the Cr-rich layer is worse.
(3) Chloride ions affects the activity of Fe atoms in the metal matrix. When chloride concentration increased, Fe^{2+} concentration in the solution and $FeCO_3$ content in the rich-Cr layer were increased and the rich-Cr layer became looser.

Acknowledgements

The research was financially supported by the National Science and Technology Major Project of China (Grant No. 2016ZX05012-001).

References

[1] D. Zeng, B. Dong, S. Shi, J. Pan, L. Cai, Effects of temperature on corrosion of N80 and 3Cr steels in the simulated CO_2 auxiliary steam drive environment, Arabian J. Sci. Eng. (2018).
[2] A. Kamari, A. Hemmati-Sarapardeh, A.H. Mohammadi, H. Hashemi-Kiasari, E. Mohagheghian, On the evaluation of Fast-SAGD process in naturally fractured heavy oil reservoir, Fuel 143 (2015) 155–164.
[3] R.T. Okwen, M.T. Stewart, J.A. Cunningham, Temporal variations in near-wellbore pressures during CO_2 injection in saline aquifers, Int. J. Greenh. Gas Cont. 5 (2011) 1140–1148.
[4] J. Zhao, G. Chen, The synergistic inhibition effect of oleic-based imidazoline and sodium benzoate on mild steel corrosion in a CO_2-saturated brine solution, Electrochim. Acta 69 (2012) 247–255.
[5] S.D. Zhu, A.Q. Fu, J. Miao, Z.F. Yin, G.S. Zhou, J.F. Wei, Corrosion of N80 carbon steel in oil field formation water containing CO_2 in the absence and presence of acetic acid, Corrosion Sci. 53 (2011) 3156–3165.
[6] L.M. Tavares, E.M.D. Costa, J.J.D.O. Andrade, R. Hubler, B. Huet, Effect of calcium carbonate on low carbon steel corrosion behavior in saline CO_2 high pressure environments, Appl. Surf. Sci. 359 (2015) 143–152.
[7] Y. Zhang, X. Pang, S. Qu, et al., Discussion of the CO_2 corrosion mechanism between low partial pressure and supercritical condition, Corrosion Sci. 59 (2012) 186–197.
[8] X. Lin, W. Liu, F. Wu, et al., Effect of O_2 on corrosion of 3Cr steel in high temperature and high pressure CO_2-O_2 environment, Appl. Surf. Sci. 329 (2015) 104–115.
[9] X. Li, Y. Zhao, W. Qi, et al., Effect of extremely aggressive environment on the nature of corrosion scales of HP-13Cr stainless steel, Appl. Surf. Sci. 469 (2019) 146–161.
[10] L. Xu, W. Bei, J. Zhu, L. Wei, Z. Zheng, Effect of Cr content on the corrosion performance of low-Cr alloy steel in a CO $_2$ environment, Appl. Surf. Sci. 379 (2016) 39–46.
[11] Y. Hua, R. Jonnalagadda, L. Zhang, A. Neville, R. Barker, Assessment of general and localized corrosion behavior of X65 and 13Cr steels in water-saturated supercritical CO_2 environments with SO_2/O_2, Int. J. Greenh. Gas Cont. 64 (2017) 126–136.
[12] G. Cui, Z. Yang, J. Liu, Z. Li, A comprehensive review of metal corrosion in a supercritical CO_2 environment, Int. J. Greenh. Gas Cont. 90 (2019) 102814.
[13] X. Li, Y. Zhao, W. Qi, J. Xie, J. Wang, B. Liu, G. Zeng, T. Zhang, F. Wang, Effect of extremely aggressive environment on the nature of corrosion scales of HP-13Cr stainless steel, Appl. Surf. Sci. 469 (2019) 146–161.
[14] B. Dong, D. Zeng, Z. Yu, L. Cai, S. Shi, H. Yu, H. Zhao, G. Tian, 'Corrosion mechanism and applicability assessment of N80 and 9Cr steels in CO_2 auxiliary steam drive, J. Mater. Eng. Perform. 28 (2019) 1030–1039.
[15] L. Xu, S. Guo, W. Chang, et al., Corrosion of Cr bearing low alloy pipeline steel in CO_2 environment at static and flowing conditions, Appl. Surf. Sci. 270 (2013) 395–404.
[16] F.F. Eliyan, F. Mohammadi, A. Alfantazi, An electrochemical investigation on the effect of the chloride content on CO $_2$ corrosion of API-X100 steel, Corrosion Sci. 64

(2012) 37–43.
[17] J. Han, J. Zhang, J.W. Carey, Effect of bicarbonate on corrosion of carbon steel in CO_2 saturated brines, Int. J. Greenh. Gas Cont. 5 (2011) 1680–1683.
[18] F. Xue, L.Y. Xu, H.Y. Jing, Y.D. Han, Corrosion behavior of mechanical clad pipe welded joints in CO_2-saturated seawater under high temperature and high pressure, Mater. Corros. 64 (2014) 544–549.
[19] M.H. Nazari, S.R. Allahkaram, M.B. Kermani, The effects of temperature and pH on the characteristics of corrosion product in CO_2 corrosion of grade X70 steel, Mater. Des. 31 (2010) 3559–3563.
[20] S. Guo, L. Xu, Z. Lei, C. Wei, M. Lu, Characterization of corrosion scale formed on 3Cr steel in CO_2 -saturated formation water, Corrosion Sci. 110 (2016) 123–133.